# Direct Observation of Mass Oscillations Due to Ablative Richtmyer-Meshkov Instability in Plastic Targets

Y. Aglitskiy,[1] A. L. Velikovich,[2] M. Karasik,[2] V. Serlin,[2] C. J. Pawley,[2] A. J. Schmitt,[2] S. P. Obenschain,[2] A. N. Mostovych,[2] J. H. Gardner,[3] and N. Metzler[1]

[1]*Science Applications International Corporation, McLean, Virginia 22150*

[2]*Plasma Physics Division, Naval Research Laboratory, Washington, D.C. 20375*

[3]*Laboratory for Computational Physics and Fluid Dynamics, Naval Research Laboratory, Washington, D.C. 20375*

(Received 18 June 2001; published 6 December 2001)

We report the first direct experimental observation of the ablative Richtmyer-Meshkov instability. It manifests itself in oscillations of areal mass that occur during the shock transit time, which are caused by the "rocket effect" or dynamic overpressure characteristic of interaction between the laser absorption zone and the ablation front. With the 4-ns-long Nike KrF laser pulse and our novel diagnostic technique (monochromatic x-ray imaging coupled to a streak camera) we were able to register a peak and a valley of the areal-mass variation before the observed onset of the Rayleigh-Taylor growth.

DOI: 10.1103/PhysRevLett.87.265001 PACS numbers: 52.57.Fg, 47.20.–k, 52.70.La

Laser target distortion due to the Rayleigh-Taylor (RT) instability remains a critical issue of the inertial confinement fusion (ICF) program [1,2]. The perturbations amplified by the RT instability grow from the so-called "seeds" which are linearly related to the nonuniformities of the target and the laser beam or the x-ray radiation field driving it. The growth rates of the RT instability have been measured in numerous experiments starting from the mid-1980s (e.g., see Refs. [3]). Much fewer experimental results are available to quantify the linear relationships between the measurable initial nonuniformities and the seed mode amplitudes. A good understanding of these relationships is necessary to ensure a reliable simulation of the overall perturbation growth, and hence, of the target performance.

Most of our knowledge in this field still comes from simulations and theory. The seed amplitudes are known to form during the early-time period that includes a shock wave transit from the front to the rear surface of the target, and a rarefaction wave transit in the opposite direction. During this time interval, the areal mass perturbations caused by all sources of nonuniformity are expected to oscillate [4–9]. The physical mechanisms driving the oscillations depend on whether the perturbations are initially at the front surface of the target (laser imprint, front surface roughness) or at its rear surface (feedout, see [9]). Here we limit ourselves to the former case, where the oscillations are caused by the "rocket effect," or the dynamic overpressure [6,8,10,11]. The oscillatory behavior is consistent with the expression for the growth rate $\Gamma$ of ablative RT instability, which has recently been established [10,11] for the case of large Froude number (low acceleration):

$$\Gamma = \left(Agk - \frac{A^2}{r_D}k^2\nu_a^2\right)^{1/2} - (1 + A)k\nu_a . \quad (1)$$

Here $g$ is the acceleration, $r_D \ll 1$ is the effective blowoff-plasma-to-ablation-front density ratio, estimated for a given perturbation wavelength $\lambda = 2\pi/k$ by the formulas given in [8,11], $A = (1 - r_D)/(1 + r_D)$ is the corresponding effective Atwood number, $\nu_a = \dot{m}/\rho_s$ is the ablation velocity ($\dot{m}$ is the mass ablation rate, $\rho_s$ is the shock-compressed target density). The main difference between (1) and all the versions of the Bodner-Takabe formula (see [12] and the references in [1–3]) is the presence of the negative term under the square root. The so-called rocket effect described by this term emerges because, as found in Ref. [12], the ablation front is an isotherm. When it is perturbed, and a part of it gets closer to the hot laser absorption zone, the temperature at the ablation front does not increase, but the temperature gradient in its vicinity, $\nabla T$, does. This, in turn, increases the local heat flux to the ablation front, $-\kappa\nabla T$, hence, the rate of mass ablation from it, thereby increasing the ablative pressure and pushing this part of the ablation front to the back. The physics of this rocket effect is explained in detail in Refs. [6,8,10]. The rocket effect rather than the mass flow through the ablation front [described by the last term in the right-hand side of (1); see Ref. [12]] determines the cutoff wavelength of ablative RT instability at high Froude numbers. Formula (1) giving the rate of exponential growth [10,11] is formally applicable even when the acceleration is low, or the wavelength is short, and such a growth does not take place [6,7]. If we substitute the value of $g = 0$, appropriate for the shock transit time, into (1), then the contribution of the square root term is purely imaginary, $\mathrm{Im}\Gamma = \pm\Omega$ where

$$\Omega = Ak\nu_a/r_D^{1/2} \quad (2)$$

is the oscillation frequency [6]. These oscillations during the shock transit time were first predicted in our simulations [5], then explained by the theory of Ref. [6] [where the term "ablative Richtmyer-Meschkov (RM) instability" was introduced], and later confirmed by many other simulations [7,8], but never actually observed experimentally.

One of the problems associated with observation of the ablative RM oscillations is their relatively low frequency. This is why these oscillations have not been detected by

  

the face-on measurements in earlier experiments [13]. For a 30 $\mu$m perturbation wavelength in a plastic target irradiated by high laser intensity, $\sim$80 TW/cm$^2$, $\nu_a \cong 1$ to 1.5 $\mu$m/ns, $r_D = 0.04$ to 0.1 [8,11], Eq. (2) predicts an oscillation half-period between 2 and 4 ns. The driving laser pulse has to be even longer than that if we want to observe the RT growth that follows the early-time RM phase. This would provide the data to validate our codes that model the early-time RT seed generation. To ensure a sufficiently long shock transit time, the plastic targets must be at least 40 to 60 $\mu$m thick. Observation of the oscillatory behavior of mass variation in such targets requires direct, high spatial resolution face-on measurements, registering relatively small changes.

We have performed experiments in this regime to observe the evolution of ablative RM instability in laser-driven targets; we present here a subset of our data to summarize our results. Our experiments were performed with the Nike KrF laser [14] ($\lambda_L = 248$ nm). The laser pulse ($\sim$1400 J in 37 overlapping beams) was focused to a spot 750 $\mu$m FWHM in diameter, with a flat central region 400 $\mu$m in diameter, producing an intensity up to $\sim 8 \times 10^{13}$ W/cm$^2$. In this set of experiments the main Nike pulse was 4 ns long, satisfying the previous pulse duration requirement. The time-average rms spatial variation for overlapped 37 beams has been measured to be less than 0.2%; hence the target is not severely distorted by the laser imprint during the shock transit time.

The diagnostic setup for the RM measurements (Fig. 1) is a modification of the Nike monochromatic x-ray imaging system based on Bragg reflection from spherically curved crystals [15]. An addition of a streak camera to this system made it possible to analyze continuous time behavior of mass variation, which is necessary to reveal the nonmonotonic evolution of the processes under study. The

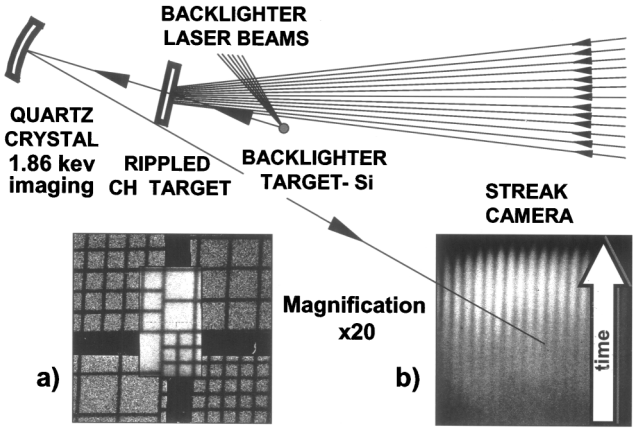


FIG. 1. General scheme of the experiment. (a) Test images of a 150-to-400 lpi composite mesh obtained on x-ray film (quadrants) and on an open photocathode of the streak camera (inset in the middle). (b) An actual streak record showing the RT growth of areal mass variation — peaks and valleys are more pronounced at late time.

energy of 12 Nike beams, $\sim$500 J, is delivered to a silicon backlighter target, producing x rays that backlight the main target for about 5 ns. The spherically curved quartz crystal selects the resonance line of the He-like Si (1.86 keV) and projects a monochromatic image of the target on the slit of an x-ray streak camera. We used quartz crystal with the cut 1011 and radius of curvature 200 mm. With magnification of 20 it makes the crystal-to-detector distance about 2 m. Our system was able to position the target image on the entrance slit of the streak camera with an accuracy that corresponds to 30 $\mu$m on the target. This setup provides spatial resolution in one relevant direction, along the wave vector of the $a_0 \sin kx$ ripple on the target surface, producing a streak record like that shown in Fig. 1(b).

Spatial resolution of the x-ray optical system was tested with the help of x-ray film as a detector and was found to be of order 6–7 $\mu$m. High throughput of the x-ray optical system allows us to magnify the images by a factor of 20 to compensate for the modest resolution of the streak camera. Despite the high magnification of the system, the overall spatial resolution was still limited by the streak camera and was estimated by test pictures of the composite mesh; see Fig. 1(a). The modulation transfer function (MTF) of the entire diagnostic system was obtained by imaging a knife-edge target and verified by imaging an undriven target with predetermined amplitude. The MTF at $\lambda = 30$ and 45 $\mu$m is 0.4 and 0.7, respectively. This test also gives us an experimental error bar for the mode amplitude measurement, which does not exceed $\pm 1$ $\mu$m in most cases.

We used 40 to 90 $\mu$m thick CH targets rippled on the front side with perturbation wavelength $\lambda = 30$ $\mu$m. This was short enough to make the oscillation half-period fit into the Nike pulse duration, but at the same time was resolvable by our diagnostics. The initial ripple amplitudes $a_0$ were approximately either 0.5 or 1 $\mu$m. This combination of perturbation wavelength and initial amplitude might not be adequate for an experiment aimed at measuring the linear RT growth: with $ka_0 = 0.1$ to 0.2, we are not far from the nonlinear stage from the very beginning. Here, however, we are primarily interested in the early-time ablative RM phase, when the perturbations of all wavelengths oscillate rather than grow exponentially, so that the higher harmonics, being initially small, remain small until the onset of the exponential RT growth. The streak records were taken with time resolution of 170 ps, sufficient for the characteristic times of interest, which are no less than 0.5 ns. The large flat top (400 $\mu$m) of the laser focal spot observed with the large field of view (500 $\mu$m) gives us more ripples available for Fourier transform analysis, thus ensuring confidence in determining the dominant mode's amplitude. We present the Fourier amplitude of mass variation [$\mu$m $\times$ g/cm$^3$] in microns, referring it to the density of solid plastic, 1.07 g/cm$^3$. This amplitude should not be confused with displacement of the ablation front. The observed mass variation also includes contributions from the rippled shock front and

the density nonuniformity between the shock and ablation fronts. Our face-on diagnostics does not allow us to evaluate any of these contributions separately. Theory and simulations indicate that the contribution of the rippled ablation front rapidly becomes dominant [5–8].

Figure 2 shows an original streak record (top) and the time dependence of its MTF-corrected Fourier component (bottom, peak-to-valley amplitude) taken from a 47 $\mu$m thick rippled target, $a_0 = 0.5$ $\mu$m, irradiated with peak intensity of $5 \times 10^{13}$ W/cm$^2$, no low energy foot. The thickness of the shaded area approximately corresponds to the experimental uncertainty. The peaks and valleys of mass variation are clearly visible on the streak record. Both light and dark stripes are less discernible between 2.5 and 3 ns, as if they were smeared in a vertical band $\sim$0.5 ns wide, indicating a minimum in the Fourier amplitude. The fast rise in mass variation following the RM-related minimum is the observed RT perturbation growth. Note that the late-time peak at about 4 ns occurs when the laser pulse is over and the target decompresses.

Figure 3 compares the results of the above shot with a thicker target (63 $\mu$m thick, $a_0 = 1$ $\mu$m) at about the same peak intensity. The shock transit takes longer for the thicker target, so the RM phase is longer by about a factor of 1.5. Hence, the RT growth starts later, and is slower due to the higher mass (lower acceleration) of the target. By the end of the laser pulse, the mass variation amplitude grows to approximately the same value as in the thinner target, despite having started from twice the initial value.

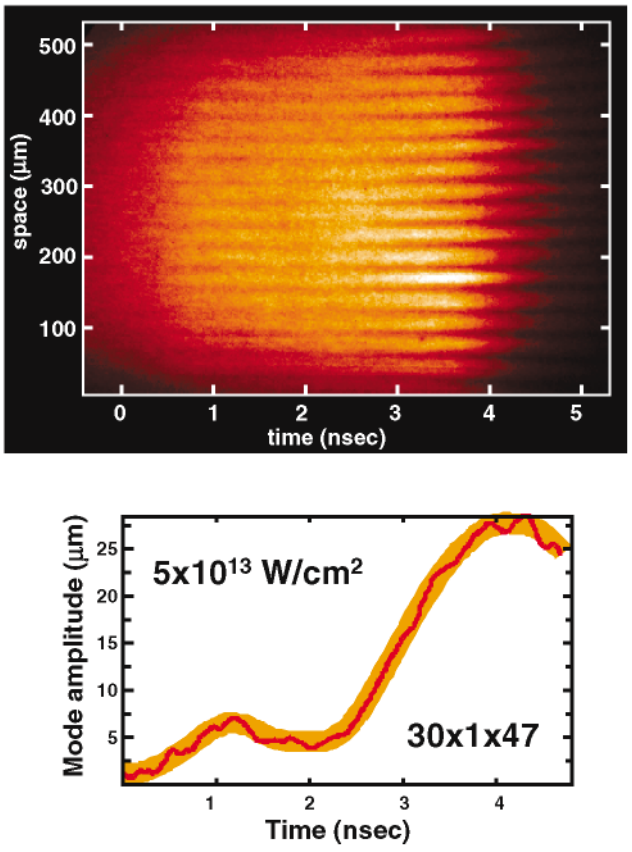


FIG. 2 (color). Streak record (top) and the peak-to-valley amplitude of the dominant Fourier mode $\lambda = 30$ $\mu$m of the areal mass variation (bottom) for a 47 $\mu$m thick target (peak-to-valley amplitude $2a_0 = 1$ $\mu$m). The minimum due to the ablative RM oscillation is clearly visible on both images.

Figure 4 shows the data obtained for the thickest target that we probed with our diagnostics, 90 $\mu$m, $2a_0 = 2$ $\mu$m. In this shot, the laser beam had a 3-ns-long, 1% foot at $t < 0$, which caused some early growth of mass variation (not shown in the figure) due to the rippled shock wave and to the perturbation of the ablation front to a $\sim$4 $\mu$m amplitude. Here the shock transit takes still longer, and the acceleration, when it starts, is lower; hence only the onset of the RT growth is seen (the laser pulse ends at 4 ns). Still, the growth of the dominant mode to the peak and its subsequent decay before the onset of RT are clearly observed. This result is compared to a simulation performed in two dimensions (2D) using the FAST2D hydrocode developed at the Naval Research Laboratory [16] (more details about the code and further references are given in Refs. [5,7]). Qualitatively, the simulation predicts exactly what we observe in all shots. Quantitative agreement is also quite reasonable.

In summary, we have observed for the first time a nonmonotonic evolution of areal mass perturbations in an ablatively driven target during the shock-rarefaction transit. The perturbations experience a half-oscillation due to so-called ablative RM instability, followed by the onset of exponential RT growth. The initial perturbations were single-mode ripples on the front surface of planar targets, corresponding to a mode of the outer surface roughness of a spherical direct-drive target. The physics of the RM oscillations excited by either surface ripples

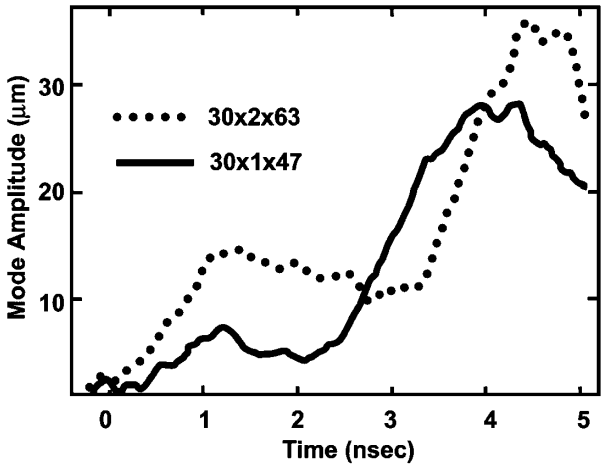


FIG. 3. Time histories of the areal mass variation (peak-to-valley) compared for 47 $\mu$m ($2a_0 = 1$ $\mu$m, $\lambda = 30$ $\mu$m) and a 63 $\mu$m ($2a_0 = 2.0$ $\mu$m, $\lambda = 30$ $\mu$m) thick targets irradiated at $5 \times 10^{13}$ W/cm$^2$(solid and dotted lines, respectively). The oscillation is followed by the RT growth, which peaks when the laser turns off and the target starts to decompress.

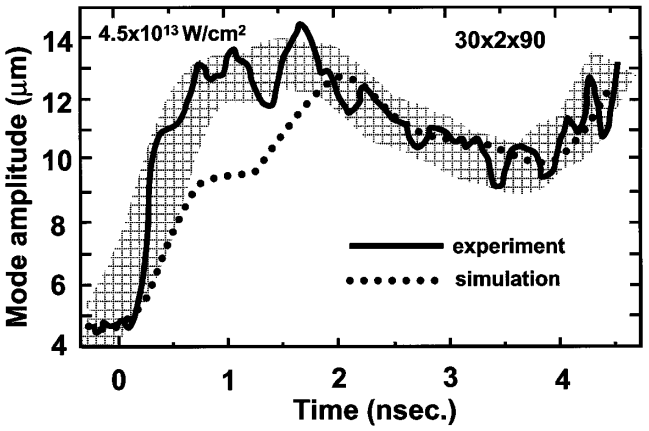


FIG. 4. Time histories of areal mass variation (peak-to-valley) for a 90 $\mu$m thick target ($2a_0 = 2$ $\mu$m, $\lambda = 30$ $\mu$m) at $4.5 \times 10^{13}$ W/cm$^2$—the RM oscillation is still observable, but only onset of the RT growth is seen. This specific shot was taken with 3 ns, 1% foot. The thickness of the shaded area corresponds to the experimental uncertainty of the mode amplitude measurement. Experiment is compared to a simulation performed with the help of FAST2D hydrocode.

or single-mode, constant phase laser beam nonuniformity is identical [5–8]. Using the former case to validate the codes, the capacity for modeling the latter can be improved.

Of course, it would be of great practical importance to observe the ablative RM oscillations in a solid deuterium target. Our present diagnostics cannot see mass variation in deuterium, which does not absorb keV x-ray quanta. There is, however, an attractive opportunity of continuing this line of experiments with deuterium-wicked plastic foam targets, as in Ref. [17]. The oscillation frequency in deuterium should be higher than in solid plastic due to its lower density [higher $\nu_a$ in (2)], making it possible to observe more than one half-cycle [5,6,8], whereas the total mass variation would be detectable via the observed changes in the areal density of the foam component.

The authors acknowledge the technical support of Nike Laser Crew and important contributions of J. Weaver, Yung Chan, and J. W. Bates. The authors are grateful to A. Faenov and T. Pikuz of VNIIFTRI, Moscow, for fruitful consultations. This work was supported by the U.S. Department of Energy, Defense Programs.

[1] S. E. Bodner *et al.,* Phys. Plasmas **5**, 1901 (1998).
[2] J. D. Lindl, Phys. Plasmas **2**, 3933 (1995); *Inertial Confinement Fusion: The Quest for Ignition and Energy Gain Using Indirect Drive* (Springer, Heidelberg, 1997).
[3] J. Grun *et al.,* Phys. Rev. Lett. **58**, 2672 (1987); C. J. Pawley *et al.,* Phys. Plasmas **6**, 565 (1999); M. Desselberger *et al.,* Phys. Rev. Lett. **65**, 2997 (1990); M. Desselberger and O. Willi, Phys. Fluids B **5**, 896 (1993); H. Azechi *et al.,* Phys. Plasmas **4**, 4079 (1997); K. Shigemori *et al.,* Phys. Rev. Lett. **78**, 250 (1997); B. A. Remington *et al.,* Phys. Fluids B **4**, 967 (1992); **5**, 2589 (1992); Phys. Plasmas **2**, 241 (1995).
[4] R. Ishizaki and K. Nishihara, Phys. Rev. Lett. **78**, 1920 (1997); Phys. Rev. E **58**, 3744 (1998); N. Matsui *et al.,* J. Plasma Phys. **61**, 43 (1999).
[5] A. L. Velikovich *et al.,* Phys. Plasmas **5**, 1491 (1998).
[6] V. N. Goncharov, Phys. Rev. Lett. **82**, 2091 (1999).
[7] N. Metzler *et al.,* Phys. Plasmas **6**, 3283 (1999); A. L. Velikovich *et al.,* Phys. Plasmas **7**, 1662 (2000); A. J. Schmitt *et al.,* Phys. Plasmas **8**, 2287 (2001).
[8] V. N. Goncharov *et al.,* Phys. Plasmas **7**, 2062 (2000).
[9] A. L. Velikovich *et al.,* Phys. Plasmas **8**, 592 (2001).
[10] J. Sanz, Phys. Rev. Lett. **73**, 2700 (1994); A. R. Piriz *et al.,* Phys. Plasmas **4**, 1117 (1997); A. R. Ririz, Phys. Plasmas **8**, 997 (2001).
[11] V. N. Goncharov *et al.,* Phys. Plasmas **3**, 1402 (1996); R. Betti *et al.,* Phys. Plasmas **5**, 1446 (1998).
[12] S. E. Bodner, Phys. Rev. Lett. **33**, 761 (1974).
[13] T. Endo *et al.,* Phys. Rev. Lett. **74**, 3608 (1995).
[14] S. P. Obenschain *et al.,* Phys. Plasmas **3**, 2098 (1996).
[15] Y. Aglitskiy *et al.,* Appl. Opt. **37**, 5253 (1998).
[16] J. P. Boris and D. L. Book, J. Comput. Phys. **11**, 38 (1973); also see *Methods in Computational Physics* (Academic Press, New York, 1976), Vol. 16, pp. 85–129.
[17] D. Sethian *et al.,* Phys. Plasmas **6**, 2089 (1999).